CHAPTER 3

Ultra-Low Voltage Eco-friendly Water Induced LiO_x/AlO_x Bilayer Dielectric Based OFET.

*Part of this work has been published as

Prashant Kumar, V. N. Mishra, and R. Prakash, "Ultralow-Voltage Eco-Friendly Water-Induced LiO_x/AlO_x Bilayer Dielectric-Based OFET," ***IEEE Trans. Electron Devices*****, vol. 70, no. 8, pp. 1–6, 2023, DOI: 10.1109/ted.2023.3285172.**

CHAPTER 3

Ultra-Low Voltage Eco-friendly Water Induced LiO_x/AlO_x Bilayer Dielectric Based OFET.

3.1 Introduction

Organic thin film transistors (OFETs) fabricated through solution-processed OSC (organic semiconductor) and dielectric layers have recently drawn the attention of researchers because of their large area and low-cost processing[34], [86]. However, the conventional silicon dioxide based OFETs have a very high voltage of operation making them unsuitable for low voltage operable wearable, portable, and IoT sensor node applications. Using an ultrathin dielectric layer or high-k dielectric are two commonly used strategies for reducing the operation voltage of OFETs. However, the ultrathin dielectric layer through the solution route has numerous disadvantages like high leakage current density, and reliability issues [87], [88]. Lithium (Li), an alkaline metal, is commonly recognized for its applications in light alloys and batteries. In past some groups have used LiO_x or combination of LiO_x as dielectric for inorganic TFTs[76], [89]. Recently we have demonstrated water processed LiO_x as dielectric for high performance OFETs [86]. Nevertheless, the subthreshold swing, on/off ratio, and operating voltage need to be improved in order to be used with Si-FET based hybrid technology [90].

Bilayer dielectrics have advantages like reduced leakage current density and a larger band gap, and can also improve the interface quality and hence other performance parameters [91], [92]. This motivated us to incorporate an additional dielectric layer of water processed AlO_x. AlO_x

film can retain an amorphous structure even after annealing at temperatures as high as 1000℃ , has a big band gap (~7-8 eV), good field strength, and high thermal stability. So it is a good choice for dielectric[93], [94]. Thus, using water-processed AlO_x as an additional layer over LiO_x can be beneficial. Because of its good amorphous nature even at high temperature, and covalent character we have kept it just before the semiconductor layer while LiO_x has been used as the first dielectric layer. In Solution processing of metal oxide based dielectrics, the commonly used solvents like 2-methoxy ethanol (2MEA) and dimethylformamide (DMF) along with other toxic additives can cause harm to the environment and human health. Water based processing of metal oxide dielectrics can solve this problem as it is environmentally friendly, cost-effective, and safe for human health than the organic counterparts. Moreover, the use of hazardous organic compounds (as additives or solvents) necessitates a higher annealing temperature and generally emits a higher number of volatile gases, which increases the roughness and film porosity of dielectric films, thereby increasing leakage current density and deteriorating OFET performance parameters[80], [95], [96]. Among the various solution process methods for the deposition of the OSC layer, the floating film transfer method (stamping of OSC film from the surface of the liquid substrate) has the advantages of large-area processing suitability and no requirement of costly instruments for film transfer. A schematic of steps involved in the FTM process is depicted in Fig. 3.1. (f) which includes three steps namely: dropping of a small amount (~ 10µL) of OSC solution over the liquid substrate, formation of the self-assembled polymer film (DPP-DTT in our case) over the surface of liquid and, stamping of the assembled film to the substrate. This method is becoming increasingly popular as it uses only a small amount of polymer solution and is suitable for flexible and large-area electronics because FTM processing hardly needs any sophisticated instrument and

minimizes the wastage of expensive polymer material so it is cost-effective too. Moreover, the use of water as a liquid substrate in place of commonly used hazardous ethylene glycol and glycerol (in the traditional FTM process) makes it more environmentally friendly[77], [79]. For the OSC layer, we employed DPP-DTT, with a highest occupied molecular orbital (HUMO) level of about -5.5 eV and a lowest unoccupied molecular orbital (LUMO) level of nearly -3.9 eV. Details on material properties, synthesis, and other characteristics of DPP-DTT have been published elsewhere [97]. In this chapter, we report a high performance -1 V operable OFET using water-induced bilayer dielectrics namely LiO_x and AlO_x. To the best of our knowledge, this is the first report investigating the performance of OFETs based on water-induced LiO_x/AlO_x bilayer dielectrics. The OSC film has been transferred using a large area suitable FTM method from the surface of the water as a liquid substrate. These DPP-DTT-based devices recorded a threshold voltage of -0.25±0.1 V, maximum saturation mobility of 0.34 $cm^2 V^{-1}sec^{-1}$, average mobility value of 0.24±0.06 $cm^2 V^{-1}sec^{-1}$, a subthreshold swing of 90±11 mV/decade, and interface trap charge density of $5.80\pm1.91 \times 10^{11}$ $cm^{-2}.eV^{-1}$. The device was operated at an ultralow voltage of -1 V. Positive bias stress (PBS) and negative bias stress (NBS) tests were also carried out for a period of 3600 sec to investigate the bias stability of these devices. A 5-week stability study has also been performed to check the ambient stability of the device. Thus, this report combines the advantages of eco-friendly water-based processing of bilayer gate dielectrics and water-based transfer of FTM film of DPP-DTT OSC instead of toxic organic solvents. This chapter is organized into five subsections including this one. The 3.2 section discusses the brief experimental steps followed by characterization details in section 3.3. The electrical characterization and extractions of parameters has been discussed in section 3.4 followed by summary of key findings in section 3.5.

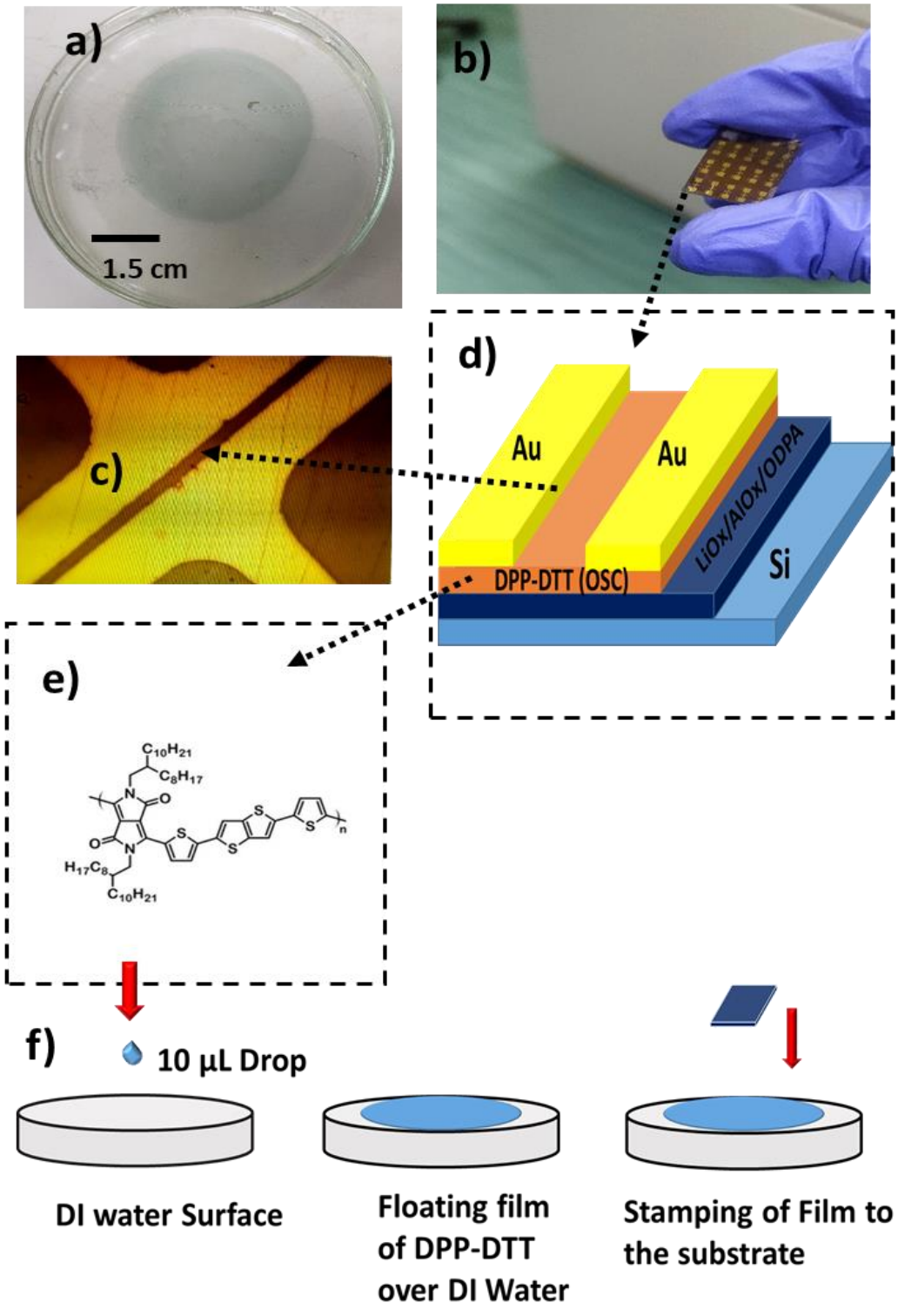

Fig. 3.1. (a) FTM film of DPP-DTT over DI water surface, (b) Image of the Device (c) Optical micrograph of the channel (d) Schematics of the Fabricated Device (e) Chemical Structure of DPP-DTT polymer, (f) Schematics representing FTM Process used.

3.2 Experimental Details

3.2.1 Materials

DPP-DTT of molecular wt. ~ 10000 was purchased from Ossila Ltd UK. Lithium Nitrate, Aluminum nitrate Nona hydrate, orthodecyl phosphonic acid (ODPA), Chloroform ($CHCl_3$), and 1,2 dichlorobenzene were procured from Sigma-Aldrich.

3.2.2 Precursor Solution Preparation

0.12 M lithium nitrate and 0.1 M Aluminum nitrate solution were prepared in Deionized (DI) water by using a magnetic stirrer for 12 hours. Thereafter the solution was aged for 24 hours. DPP-DTT was dissolved in a solution that consisted of chloroform and chlorobenzene in the volume ratio of 8:2 using a concentration of 10 mg/mL. All three solutions were filtered using a 0.22 µm syringe filter to remove the undissolved particles.

3.2.3 Device Fabrication Steps:

p-type Silicon substrates were sliced into segments of 2 cm × 1.5 cm and used as back gate contact. The diced silicon substrates were cleaned using acetone, and 2-propanol by ultrasonication for 15 min each before thoroughly rinsing using DI water. The cleaned silicon substrates were then dried under a Nitrogen environment. Thereafter the diced silicon substrates were subjected to plasma cleaning in an oxygen environment (60 W) for 10 min. The plasma cleaning process enhances OH^- ions on the surface which help in good surface adherence of the solution coated film. Next the 0.12 M Lithium nitrate solution was spin coated on the plasma cleaned silicon substrate at 4000 rpm for 35 sec and heated at 100℃ for 10 min to remove the solvent before being annealed at 300℃ for 1 hour so as to emit the gaseous byproducts (when not done it may affect the surface roughness of second layer by increasing

film porosity). Then the 0.1M Aluminum nitrate solution was spin coated as a second layer over LiO_x film at 5000 rpm for 30 sec before being annealed at 300℃ for 2 hours.

For self-assembled monolayer (SAM) modification, the coated dielectric film was dipped in 1 mM ODPA (orthodecyl phosphonic acid) solution in ethanol for ~ 6 hours. Then the SAM treated samples were ultrasonicated for 15 minutes using ethanol in order to remove the extra and loosely bound SAM molecules. For the OSC layer, we have used DI water-filled Petri dish as the film transfer medium. Thereafter the 10 µL of DPP-DTT was dispensed over the still DI water surface kept in a Petri dish. The thickness of FTM transferred DPP-DTT film was 26±4 nm measured using Filmetrics FV 20. The picture of the floating film of DPP-DTT obtained in Petri dish and schematics of steps involved in the FTM process are shown in Fig. 3.1. (a) and (f) respectively. Source drain electrodes (with channel dimensions of 1000µm/30µm) were deposited using metal masks (purchased from Ossila Ltd UK) via a thermal evaporation unit (124AD from Hind Hivac). Firstly, a chromium adhesion layer of ~ 2 nm was deposited which was followed by the deposition of ~ 54 nm gold layer at the rate of ~ 0.03 nm/s (chamber pressure of ~ 10^{-6} mbar).

3.3 Characterization

3.3.1 AFM and Surface Morphologies of the Dielectric Film and Semiconducting Layer

The surface morphologies of the dielectric film and water-lifted DPP-DTT OSC layer has been analyzed using atomic force microscopy (NTEGRA Prima from NDMDT Services, Netherlands) in tapping mode over the area of ~ 5 µm × 5 µm in each case. Fig. 3.2 (a), (b), (c), and (d) represents 3D AFM images of LiO_x, LiO_x/AlO_x, LiO_x/AlO_x/ODPA, and LiO_x/AlO_x/ODPA/DPP-DTT film over the silicon substrate (p++). The root mean square (rms) roughness (R_q) of the water-induced LiO_x film was ~ 1.2 nm whereas LiO_x/AlO_x film has a

roughness of ~ 0.15 nm. So the water-induced AlO_x has a smoother surface than LiO_x thus more suitable for dielectric interface as the smother dielectric surface reduces scattering and trap centers thereby enhancing carrier mobility and overall device performance[86], [96]. The ODPA-treated film has slightly increased roughness (R_q) of ~ 0.22 nm but is still in the same range. Generally, a desirable criterion for the solution-processed insulating materials to be employed as gate dielectrics in OFETs is that the surface roughness should be as small as possible. A dielectric surface with minimum roughness reduces scattering centers for charge carriers and interface charge traps, resulting in a superior OSC-dielectric layer interface that is advantageous for the charge transport phenomenon. Such low rms roughness of the dielectric layer will inevitably lead to the formation of a good interface with smaller subthreshold voltage and improved carrier mobility. Moreover, the smoother dielectric layer will facilitate the growth of a high-quality OSC layer which will in turn lead to high-performance OFET with good stability[96]. The rms roughness (R_q) of the water-lifted FTM film of DPP-DTT over the ODPA-treated LiO_x/AlO_x dielectric was found to be ~ 1.76 nm.

3.3.2 Bandgap calculation of Dielectric layers.

The band gap of the bilayer dielectric was calculated using the UV-vis analysis as shown in Fig. 3.3. (a) and (b). Separate UV-vis analysis of LiOx and bilayer LiOx/AlOx film were carried out by Jasco 770 UV spectrophotometer using quartz substrates. The band gap of LiO_x (annealed at 300℃) was found to be ~ 5 eV, which is slightly smaller (but still in the same range) than the previously reported value of ~5.5 eV for LiO_x[76], while the bilayer of LiO_x/AlO_x (annealed at 300℃) showed a band gap of ~ 5.6 eV. A higher band gap ($\geq$ 5.5 eV) is required for a reduction in leakage current[98].

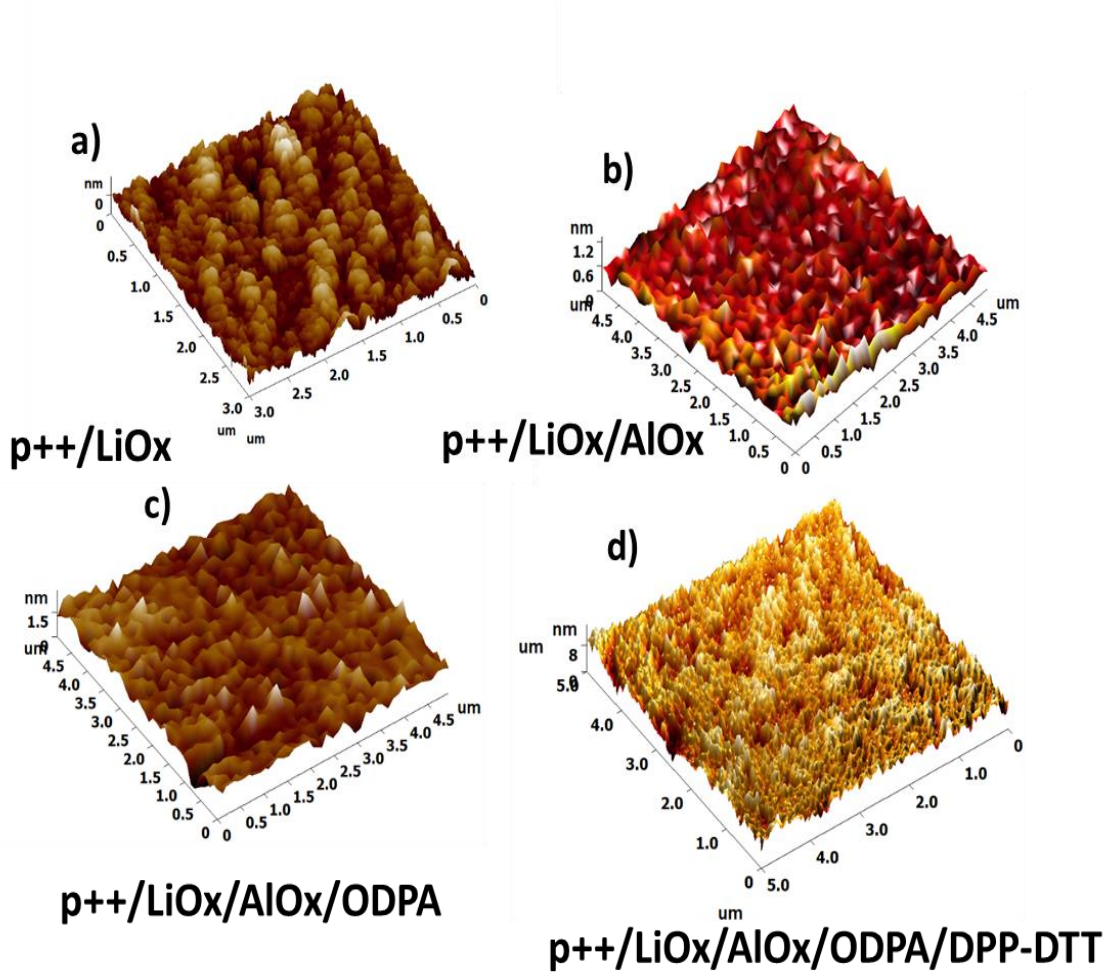

Fig. 3.2. (a) AFM image of water induced LiOx Film over p++ Si (b) AFM image of Water induced AlOx Film over LiOx/ p++ Si,(c) AFM image of ODPA treated AlOx Film over LiOx/ p++ Si, and (d) AFM image of Water lifted DPP-DTT on the surface of ODPA treated bilayer AlOx/LiOx (x and y axis values are in nm).

3.3.3 Dielectric Characterization.

In order to investigate the insulating properties of LiO_x/AlO_x bilayer dielectric metal insulator Semiconductor (MIS) structures were fabricated with gold top contacts. The leakage current behavior of the LiO_x, and ODPA-treated bilayer LiO_x/AlO_x is shown in Fig. 3.3 (c) The leakage current density ($J_{Leakage}$) has decreased in the final combination by a factor of ~10. The leakage current densities of LiO_x/AlO_x/ODPA (~2.5×10^{-9} A/cm^2 at -1 V) film have been much lower

than the LiO_x (~ 3.7×10^{-8} A/cm^2 at -1 V) dielectric layer as shown in Fig. 3.3 (c) The range of leakage current through the dielectric layer is suitable for low-voltage OFET fabrication[36]. The C-f characteristics of the above MIS structures were also studied as shown in Fig. 3.3 (d). The effective dielectric capacitance (C_i) is formed by the series combination of LiO_x, AlO_x, and ODPA films. The overall capacitance densities of the hybrid dielectric film of LiO_x/AlO_x/ODPA have reduced from 378 (±24) nF/cm^2 of LiO_x to 195 (±15) nF/cm^2 at 1 kHz. Using Filmetrics FV 20, the thickness of the LiO_x layer was found to be 19±2 nm, and bilayer LiO_x/AlO_x was computed to be 35±2.8. Based on this data and using a series capacitance combination for both layers the effective dielectric constant of LiO_x was ~ 7.94 and that of LiOx/AlOx was ~ 7.2 at 1 KHz. This value is comparable to earlier reported values [76]. Since low-frequency Capacitance behavior is also important for OFET characterization it was measured at different frequencies (below 1 KHz) using HP 4884A LCR meter and plotted in Fig 3.4 (d).

3.4 Results and Discussion

The fabricated unencapsulated LiO_x/AlO_x/DPP-DTT OFETs were characterized in an open environment using Agilent B1500A Semiconductor analyzer. All characterizations were carried out at room temperature and in dark. Fig. 3.4 (b) represents the transfer characteristics of the representative OFET measured in step of V_{DS} = -1 V. As evident from transfer characteristics, the DPP-DTT-based OFET shows typical hole characteristics. We can see clear saturation of drain current in Fig. 3.4 (a) which is representing the output characteristics of DPP-DTT based OFET. Threshold voltage and mobility calculations were done by fitting a line of maximum slope to the square root of the drain current and V_{GS} curve. Subthreshold

swing (SS) has been determined by using the reciprocal of the maximum slope obtained through a semi-log plot of the drain current. The mobility (μ), interface trap density (N_{it}), and subthreshold swing (SS) have been computed with the following set of equations[96]:

$$I_D = \frac{\mu C_i W}{2L}(V_{GS} - V_{TH})^2 \qquad (3.1)$$

$$SS = \left(\frac{dlog(I_D)}{dV_{GS}}\right)^{-1} \qquad (3.2)$$

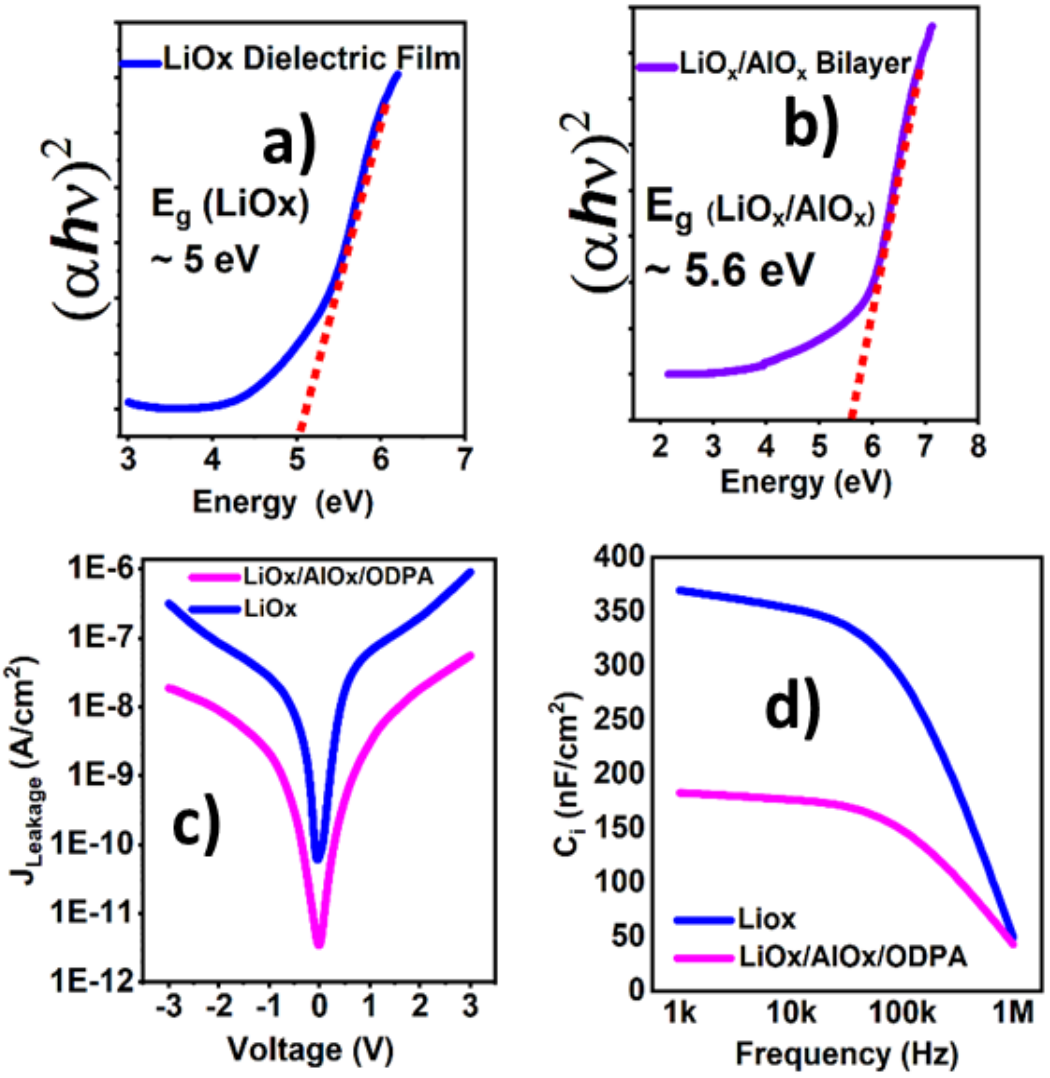

Fig. 3.3. (a) Tauc Plot of Water induced LiOx, (b) Tauc Plot of Water induced LiOx/AlOx Bilayer, (c) Leakage current Density of bare LiOx, and ODPA treated LiOx /AlOx (d) Capacitance density of LiOx and LiOx/AlOx/ODPA.

$$N_{it} = \left(\frac{loge \cdot SS}{\frac{kT}{q}} - 1 \right) \frac{C_i}{q} \qquad (3.3)$$

$$\mu = \frac{2L}{W} \left(\frac{\partial I_D}{\partial V_{GS}} \right)^2 \qquad (3.4)$$

Where C_i, I_D, V_{GS}, q, W, L, and kT represent capacitance per unit area of the gate dielectric, drain current, gate-source voltage, the charge on an electron, channel width, channel length, and, thermal energy respectively. The OFET transfer characteristics measured for 12 devices recorded average mobility of 0.24±0.06 $cm^2\ V^{-1}sec^{-1}$, maximum mobility of 0.34 $cm^2\ V^{-1}sec^{-1}$, On/off ratio of ~10^5, Subthreshold swing of 90±11 mV/decade, the trap charge density of 5.80±1.91 × 10^{11} $cm^{-2}.eV^{-1}$, and with negligible hysteresis indicating the formation of good dielectric semiconductor interface. The Device exhibited negligible hysteresis of ~ 0 V (forward and reverse sweep of transfer characteristics shown in Fig. 3.4 (c)) which is indicative of the formation of good quality dielectric semiconductor interface with low trap density. The obtained value of N_{it} (~ 10^{11} eV^{-1} cm^{-2}) also supports this. The obtained parameters for these devices have been compared with our previous report of water processed LiO_x based DPP-DTT OFET[86] in table 2. The obtained parameters have improved in bilayer LiO_x/AlO_x based DPP-DTT OFETs. Improvement in threshold voltage, Subthreshold swing, and mobility can be attributed to the smoother dielectric surface of AlO_x, and the formation of a good dielectric OSC interface. While improvement in the on/off ratio can be attributed to the use of bilayer dielectrics. Additionally, water-based processing can be attributed to the creation of a non-porous and smoother dielectric surface as organic solvents have higher annealing temperatures leading to increased porosity and surface roughness at higher temperatures [96].

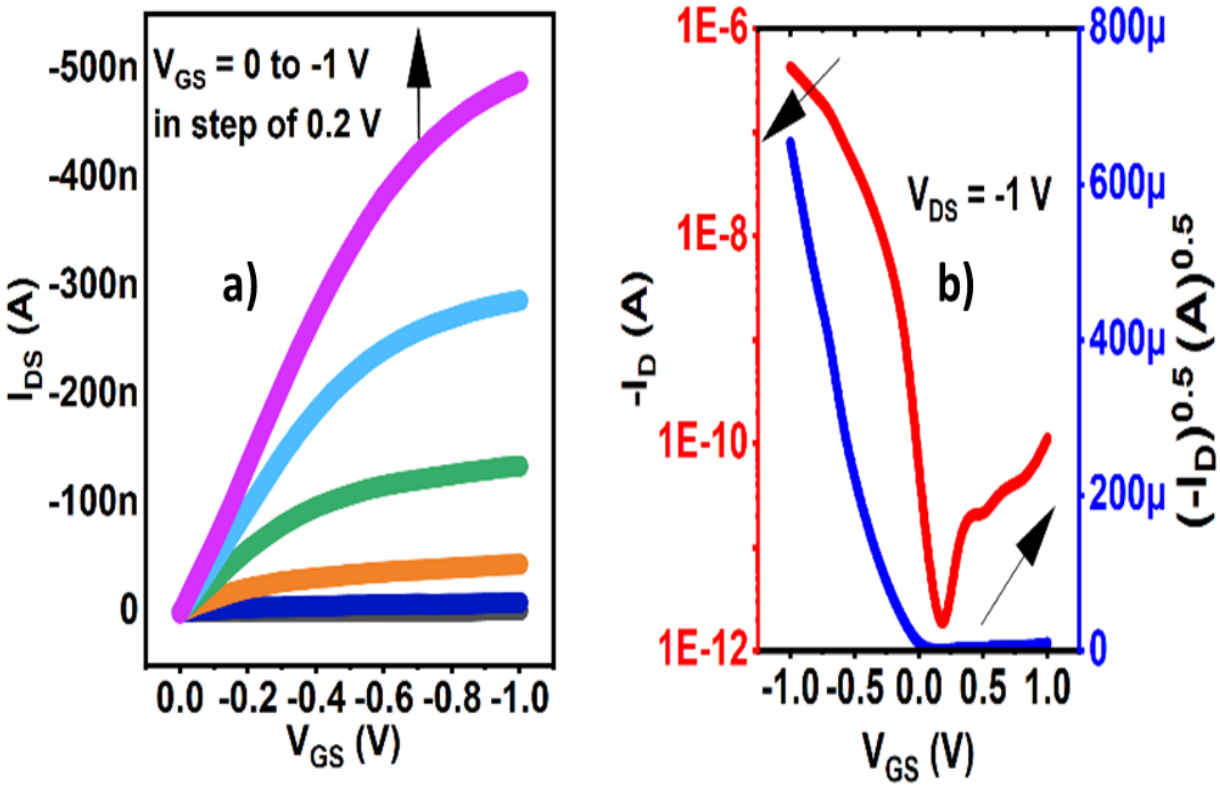

Fig. 3.4. (a) Output Characteristics,(b) transfer characteristics of LiOx/AlOx/DPP-DTT OFET.

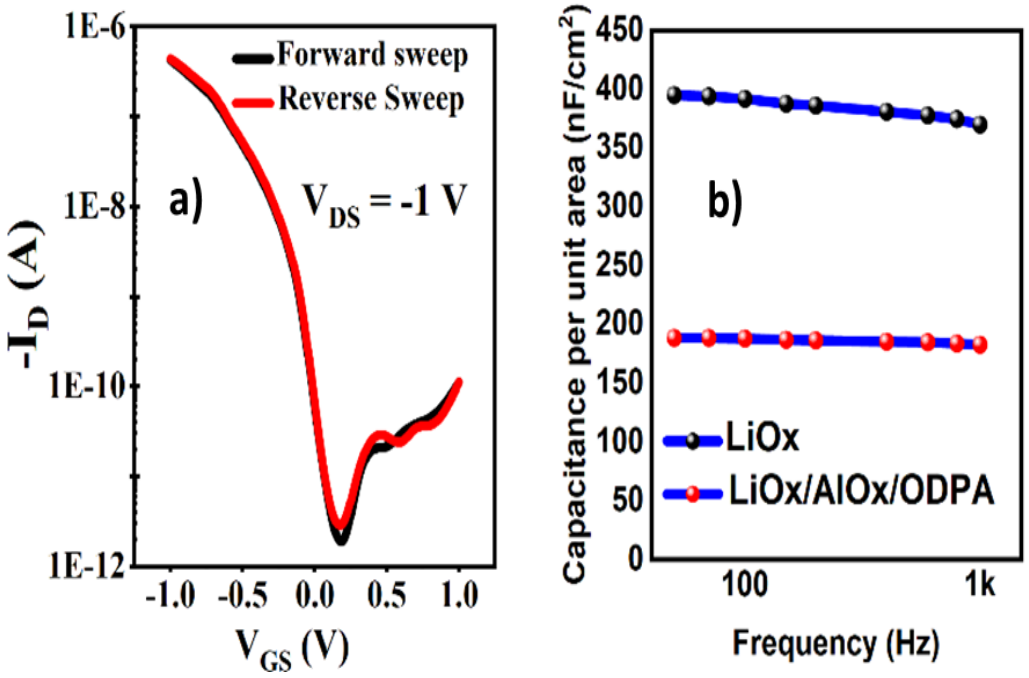

Fig. 3.5. (a) and Hysteresis characteristics of LiOx/AlOx/DPP-DTT OFET and (b) Areal capacitance of MIS at lower frequency.

Table 3.1 compares performance parameters and operating voltage of some of the reported OFETs where SC stands for spin coating and V for vapor deposition technique.

TABLE 3.1

COMPARISON OF PRESENT WORK WITH EXISTING REPORTED OFETS

Structure	μ_{max} ($cm^2 V^{-1}sec^{-1}$)	I_{on}/I_{off}	SS (mV/decade)	V_{TH} (V)	Deposition method (OSC/Dielectric)	V_{GS} (V)	Ref.
HfO2/PVA/TIPS	0.69	10^3-10^4	-	-0.58	SC/V/SC	-10	[34]
LiOx/DPP-DTT	0.16	10^4	186	-1.12	W-FTM/SC	-2	[86]
TiO_2/HfO_2/P3HT	0.10	10^3	500	-0.159	FTM/SC/SC	-1.5	[99]
HfO_x/Pentacene	0.42	10^4	370	-1.1	V/SC	-4	[100]
HfO2/PVP/TIPS	0.11	10^5	810	0.08	V/SC/SC	-10	[33]
ZrO_x/PBTTT C14	0.18	10^5	115	-0.75	SC/SC	-3	[32]
LiO_x/AlO_x/DPP-DTT	0.34	10^5	90	-0.26	W-FTM/SC	-1	This Work.

The DC bias experiment was carried out under a dark and ambient atmosphere. In order to carry the positive bias stress (PBS) and negative bias stress (NBS) experiment, we applied a stress voltage of V_{GS} = 1 V V_{GS} = -1 V respectively for the different intervals of time under dark and ambient conditions and I_D-V_{GS} characteristics were recorded. Fig. 3.5 (a), and (b)

represent the characteristics of the device under different NBS and PBS duration respectively. The device showed a threshold voltage shift of ~ - 0.06 V and ~ 0.08 V for negative and positive bias stress respectively after 3600 sec. The threshold voltage shift for NBS and PBS is plotted at different intervals of time in Fig. 3.5 (c).

A test to check the current bias stability was also carried out at V_{DS} = 1 V and V_{GS} = -1 V. As shown in Fig. 3.5 (d) the normalized current decay has been plotted which records a decay of ~ 10 % in drain current for 3600 sec. The normalized current decay curve was fitted using equation (5) [34]. The obtained values of τ and β were 1.023×10^8 sec and 0.288 where τ represents the trapping time constant of charge carriers to fill the trap at the interface, while β (a temperature-dependent parameter) generally signifies the width parameter of the interface trap distribution.

$$\frac{I_{DS}\ (t)}{I_{DS}\ (0)} = \exp\left(-2\left(\frac{t}{\tau}\right)^{\beta}\right) \qquad (3.5)$$

Such good performance to NBS and PBS can be attributed to the formation of a good interface which is supported by the N_{it} value of ~ 10^{11}, a large trapping time of ~10^8 sec, and air stability of DPP-DTT[101].

We also tested the ambient stability of the device for 5 weeks by keeping the device in ambient. For this, the transfer characteristic of the device was measured at V_{DS} = -1 V every 7^{th} day for 5 weeks. The temperature of the surrounding varied between 25±3 ℃ and humidity ~55 %. The transfer curve of the representative device taken at an interval of one week has been plotted in Fig. 3.6 (a). The variation in threshold voltage, mobility, subthreshold swing, and on/off ratio has been plotted in Fig. 3.6 (b) and (c). This stability can be attributed to the air stability

of DPP-DTT [101] and the hydrophobic nature of ODPA SAM treatment. Such low voltage operable OFETs with good subthreshold swing can be utilized for IoT based sensor nodes, low voltage phototransistors, Si-FET based hybrid technology or Gas Sensors. Further with use of polymer additives the device can be optimized for fabrication on wearable substrates. However, this requires lots of challenges like flexibility issues with oxide dielectrics.

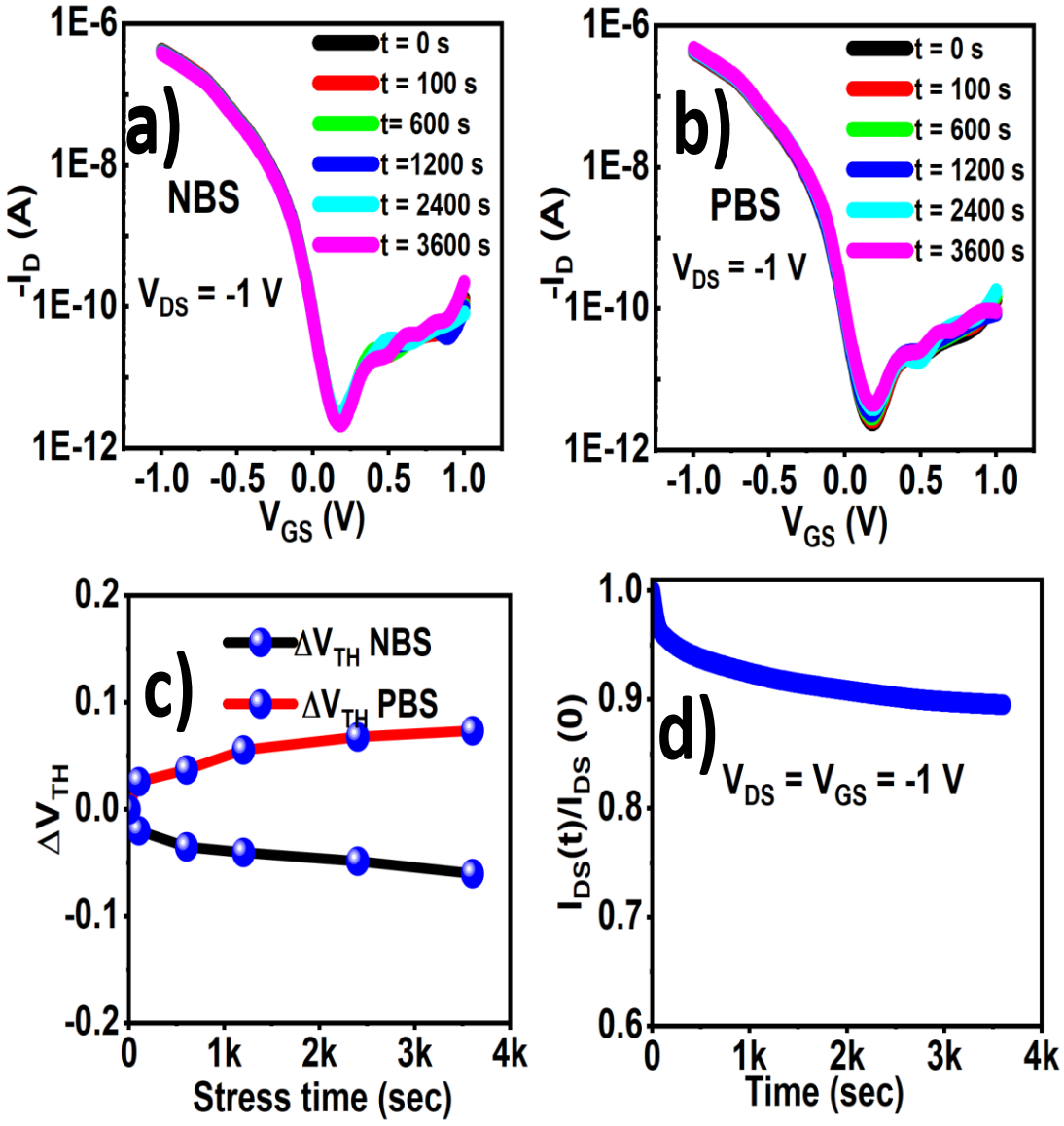

Fig. 3.6. Stress Bias Stability Study of DPP-DTT OFET (a)Negative bias stress, (b)Positive bias Stress at different intervals of time,(c) Shift in threshold Voltage on NBS and PBS, and (d) Drain current Decay over 3600 Sec.

Table 3.2

Comparison of LiOx-based and Bilayer LiOx/AlOx DPP-DTT OFET

V_{TH} (V)	μ_{sat} (cm^2 $V^{-1}sec^{-1}$)	SS (mV/decade)	N_{it} (10^{11} $cm^{-2}.eV^{-1}$)	I_{ON}/I_{OFF}	ref
-1.12 (±0.3)	0.14 (±0.035)	186 (±15)	46.3 (±04.2)	~10^4	[86]
-0.25±0.1	0.24±0.06	90±11	5.80 (±1.92)	~10^5	This work

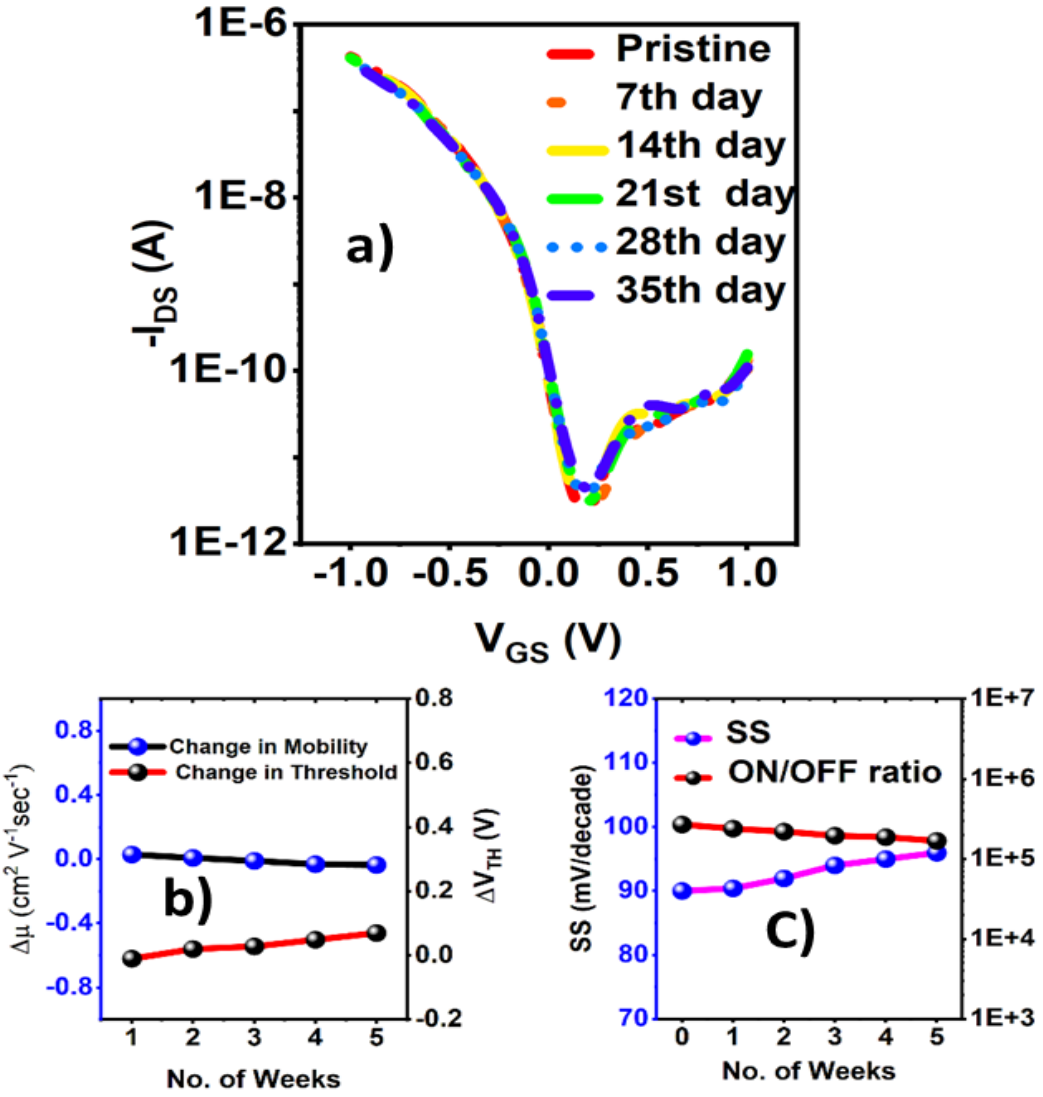

Fig. 3.7. Ambient stability Study of DPP-DTT based OFET over 5 weeks a) Transfer Characteristics of DPP-DTT OFET over 5 weeks (b) Variation in Mobility and Threshold Voltage of DPP-DTT OFET over 5 Weeks (c) Variation in Subthreshold swing (SS) and ON/OFF ratio over 5 weeks.

3.5 CONCLUSION

In summary, this report demonstrates bilayer eco-friendly water-induced LiO_x and AlO_x dielectric-based high-performance and ultra-low voltage operable (-1 V) OFETs using DPP-DTT OSC film. The average mobility of OFETs from transfer characteristics observed for 12 devices was 0.24±0.06 $cm^2 V^{-1}sec^{-1}$, with maximum mobility of 0.34 $cm^2 V^{-1}sec^{-1}$. Moreover, the On/off ratio of ~10^5, the Subthreshold swing of 90±11 mV/decade, and the trap charge density of 5.80±1.91 × 10^{11} $cm^{-2}.eV^{-1}$ were recorded. The DPP-DTT film has been transferred using the FTM method. The liquid substrate in the FTM to transfer OSC film was water. The FTM method is suitable for large-area processing of OSC film without the need for any sophisticated instrument. Because of its large area processing suitability, this work can be extended to flexible substrates. Hence, the water-processed bilayer dielectric (LiO_x/AlO_x) based ultra-low voltage operated (-1 V) and FTM transferred DPP-DTT OFET has the potential to be a competitive alternative for use in large-area electronics that are inexpensive, power-efficient, and environmentally safe to process, in the future.